energy&fuels

pubs.acs.org/EF

Article

ϕ-Sensitivity of Gasoline/Oxygenate Blends in an Advanced Compression Ignition Engine

Jonathan A. Martin,* Matthew A. Ratcliff, Mohammad J. Rahimi, Jonathan L. Burton, Petr Sindler, Cameron K. Hays, and Robert L. McCormick

Cite This: *Energy Fuels* 2023, 37, 12243–12258

Read Online

ACCESS | Metrics & More | Article Recommendations | Supporting Information

ABSTRACT: Advanced compression ignition (ACI) engines have shown the potential to improve internal combustion engine efficiency while drastically reducing levels of nitrogen oxides (NO_X) and particulate matter, including soot, in the exhaust. However, achieving high loads and control over ACI engines requires improvement of fuel ϕ-sensitivity relative to standard gasoline. Ideally, improving fuel ϕ-sensitivity will go hand-in-hand with reducing fuel carbon intensity. This study identifies three potential low-carbon fuels that can be blended with gasoline for use in ACI engines: methyl pentanoate, 1-pentanol, and 2-pentanol. These fuels have been tested in approximately 30% blends with gasoline at three different speed/load conditions in a medium-duty CI engine. Two different ϕ-sensitivity metrics were developed. The first metric ("Type 1") evaluates the change in ignition timing with respect to the start-of-injection timing of the final injection in a multi-pulse ACI injection schedule. According to this metric, 1-pentanol increased ϕ-sensitivity by 57%, 2-pentanol by 56%, and methyl pentanoate by 21% over the baseline gasoline. The second metric ("Type 2") determines how far combustion phasing, in terms of degrees of engine rotation, could be advanced before a limit of engine ringing intensity was reached. According to this metric, 1-pentanol allowed 1.03° of advance, 2-pentanol 0.83°, and methyl pentanoate only 0.20°. For both metrics, these results are the average of three speed/load engine conditions, and for the methyl pentanoate, the standard deviation across these three conditions was larger than the average ϕ-sensitivity improvement. This leads to the conclusion that methyl pentanoate does not offer any significant ϕ-sensitivity benefits, while the pentanols do. Both 1-pentanol and 2-pentanol are thus fuels of interest for further study as low-carbon blendstocks for ACI engines.

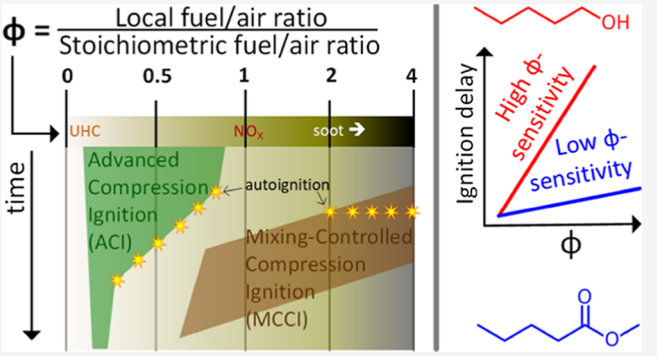

INTRODUCTION

The direct carbon dioxide (CO_2) emissions generated from the transportation sector are a principal contributor to climate change.[1] In light-duty (LD) vehicles, internal combustion engines (ICEs) have begun to be replaced by electric powertrains, and this trend is expected to rapidly increase in the next decade.[2] However, progress has been slower for heavy-duty (HD) vehicles,[2] which face higher technical and logistical barriers to electrification.[3] Demand for road freight transport via HD vehicles is only expected to increase, and it is thus imperative to reduce the net CO_2 emissions of the fuels that power these vehicles.[4] Thankfully, there are many potential carbon-neutral fuels for these vehicles, e.g., biofuels, synthetic hydrocarbons, and direct solar fuels.[5]

The HD vehicle market is dominated by compression-ignition (CI) engines, as opposed to the spark-ignition (SI) engines which power most LD vehicles.[6] The standard components of a CI engine are depicted in Figure 1a. Conventional CI engines utilize the combustion mode of mixing-controlled CI (MCCI).[7] In conventional diesel MCCI, fuel is injected very late in the compression (2nd) stroke of the 4-stroke CI engine cycle, which is depicted in Figure 1b. There is little time for fuel and air to mix before ignition, and most of the fuel will burn in a two-stage process: first by rich premixed combustion and then by diffusion combustion.[8] This creates high levels of nitrogen oxides (NO_X) and particulate matter (PM), and thus, MCCI engines must be outfitted with selective catalytic reduction (SCR) systems to reduce NO_X emissions and diesel particulate filter (DPF) systems to reduce PM emissions.[9] Several low-net-carbon substitutes for petroleum-based diesel fuel have been researched that can improve NO_X and PM emissions,[10] but not to the degree that SCR and DPF systems can be eliminated.

Received: May 3, 2023
Revised: July 7, 2023
Published: July 26, 2023

https://doi.org/10.1021/acs.energyfuels.3c01537
Energy Fuels 2023, 37, 12243−12258

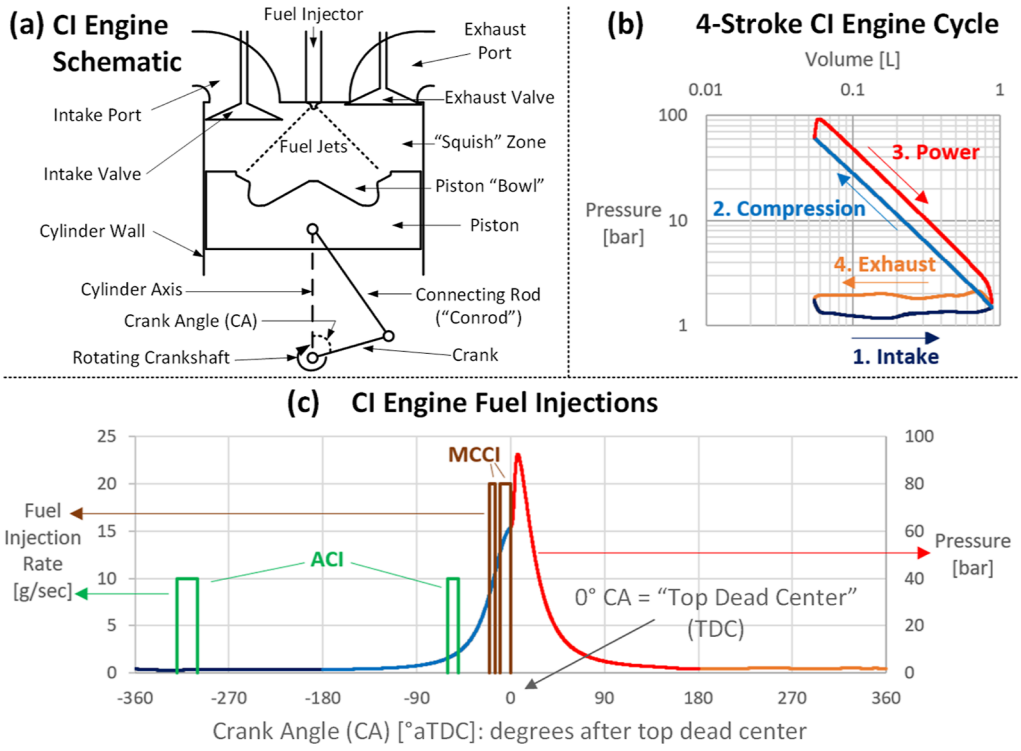

Figure 1. (a) Key components of a CI engine referenced throughout this paper. (b) Typical 4-stroke CI engine cycle shown on a log−log pressure−volume (P−V) diagram. (c) Fuel injection schedules for ACI and MCCI combustion modes, along with typical cylinder pressure. The key variable in the injection schedule is the CA between the crank and cylinder axis, measured in units of degrees after top dead center (°aTDC).

A typical MCCI injection strategy is compared with an example of advanced CI (ACI) injection strategy below in Figure 1c. This is just one example of many different injection strategies that fall under the wide scope of ACI. A common theme of all ACI strategies is that injection is "advanced", i.e., moved earlier in the engine cycle relative to MCCI.[11] This allows for more time for fuel and air to mix before ignition and increases the portion of the charge that achieves a lean fuel/air mixture prior to combustion.[11] This results in engine-out NO_X and PM emissions that are, in some cases, already low enough to meet emission standards without the need for SCR or DPF on the tailpipe.[12] Unlike MCCI, ACI can utilize fuels with a high octane number (ON), such as gasoline[13] and fuels not typically used in CI engines. However, ON and the associated standard fuel metrics of research ON (RON), motor ON (MON), and octane index (OI) were developed for SI engines and do not give a complete evaluation of a fuel's suitability for ACI.[14] Notably, the demand for gasoline may fall as LD vehicles transition to being electric, making gasoline a potentially economical fuel for medium-duty (MD)/HD applications.

One of the earliest ACI modes developed was homogeneous charge CI (HCCI), in which injection is highly advanced or mixed with intake air upstream of the intake valve, and all fuel is evenly distributed throughout the cylinder upon ignition.[15−17] Although multiple fuel performance metrics have been developed to aid in HCCI fuel/engine design,[18,19] HCCI engines have proven difficult to control over the wide range of operating conditions necessary for commercial engines.[17] Other ACI combustion modes, including those used in this study (see Figure 1c and following sections), allow for greater control by including later (more "retarded") injections producing greater fuel/air stratification.[11,20,21] The local fuel/air ratio (F/A) is commonly measured in terms of the equivalence ratio or ϕ (phi), in which $\phi = 1$ is equal to the stoichiometric fuel/air ratio $(F/A)_s$.[22] Areas where $\phi > 1$ are rich (excess fuel), and areas where $\phi < 1$ are lean (excess oxygen), as calculated by the following equation[22]

$$\phi = \frac{(F/A)_{\text{actual}}}{(F/A)_s} \tag{1}$$

In ϕ-stratified ACI, the mostly lean premixed charge will undergo a series of "sequential autoignition" events proceeding through the gradient of ϕ, without larger propagating flame structures seen in conventional SI and CI engines or the volumetric combustion seen in HCCI.[23] By utilizing different ACI modes at different operating conditions, a "multi-mode" ACI strategy can produce controllable, low-NO_X and low-PM combustion over the entire range of necessary engine operating conditions. However, fuel performance metrics that can be applied to these combustion modes have not yet been developed.[14]

The phasing of this sequential autoignition process will depend on the fuel's "ϕ-sensitivity", i.e., the sensitivity of ignition delay to the equivalence ratio of the charge. With a low ϕ-sensitivity fuel, autoignition will occur relatively simultaneously throughout the entire premixed charge, even if there is a significant stratification of ϕ. This is undesirable because it will generate high maximum pressure rise rates (MPRRs), which are the source of combustion noise and damaging "knock" in CI engines. On the other hand, a high ϕ-sensitivity fuel will slow down the sequential autoignition process, with autoignition at different local equivalence ratios being relatively further spaced out in time. This will reduce the maximum rates of heat release, thus reducing MPRR and knock. This allows ACI to be used at higher loads and higher compression ratios, making ϕ-sensitivity an important property to quantify in ACI fuels.[24]

https://doi.org/10.1021/acs.energyfuels.3c01537
Energy Fuels 2023, 37, 12243−12258

In this paper, the ϕ-sensitivity of several fuels and their resultant combustion performance will be evaluated in a MD research engine. The fuels selected are mostly gasoline or a gasoline surrogate, blended with oxygenated compounds that could potentially be made from low-net carbon feedstocks. This work takes place as part of the larger co-optimization of engines and fuels (co-optima) program funded by the U.S. Department of Energy.

The aim of this work is to confirm the ϕ-sensitivity of fuels that have been hypothesized to be highly ϕ-sensitive in simulations and/or bench experiments but have not been confirmed as such in engines operating on ACI. By focusing on oxygenated fuel candidates, the authors seek viable fuels that can not only displace fossil fuels and decarbonize the HD transportation sector but also enable high-efficiency ACI strategies that will greatly reduce harmful NO_X and soot emissions. While only a select few fuel candidates are the focus of this study, it is our intent that the methods developed can be applied in the wider research community to analyze other potential ACI fuels.

EXPERIMENTAL SECTION

Fuels. The design of the study's fuels started with the selection of the blendstocks for oxygenate blending (BOBs), which are detailed in Table 1. First, a petroleum distillate gasoline BOB was selected: the RD-587 BOB, which makes RD-587 gasoline when mixed with 10% vol ethanol. RD-587 is the baseline reference gasoline of choice for the co-optima program and represents the "regular-grade" 87-octane E10 gasoline commonly available at pumping stations in the US today. Then, six-component surrogate BOBs were designed in an iterative process to match the RON of RD-587 as closely as possible when blended with oxygenates. BOB-2B was the successful result of this process, with BOB-2C designed with higher ONs than BOB-2B for blending with particularly low-octane oxygenates.

Table 1. Composition of BOBs[a]

BOB name	RD-587 BOB (real gasoline)	BOB-2B (surrogate)	BOB-2C (surrogate)
abbreviation	"87"	"2B"	"2C"
n-heptane (Paraffins) [vol %]	17.0	16.0	2.9
isooctane (iso-paraffins) [vol %]	36.4	48.0	60.0
toluene (aromatics) [vol %]	26.8	10.0	10.7
1,2,4-trimethyl-benzene [vol %]	–	16.0	16.4
tetralin [vol %]	–	3.0	2.9
(naphthenes) [vol %]	13.5	–	–
1-hexene (olefins) [vol %]	6.4	7.0	7.1

[a]Paraffins, iso-paraffins, aromatics, naphthenes, and olefins volume percentages from DHA analysis of RD-587 BOB. Target volume percentages for surrogate BOBs.

The low-net-carbon oxygenates identified for this study are detailed in Table 2. While ethanol was included as the most prevalent low-net-carbon oxygenate, the other three were selected to test their expected varying ϕ-sensitivity while sharing a common five-carbon chain. The fuel property ϕ-sensitivity is associated with intermediate-temperature heat release (ITHR) during the early phases of autoignition, and ITHR in turn is the result of a growing pool of formyl radicals. Gasoline range paraffinic hydrocarbons, especially straight-chain or n-paraffins comprising multiple methylene ($-CH_2-$) moieties, are a significant source of formyl radicals and thus exhibit both ITHR and low-temperature heat release (LTHR). However, the ONs of *n*-paraffin decrease rapidly with increasing chain length. For example, the RON of *n*-pentane is 62, *n*-hexane has a RON of 25, and *n*-heptane is defined as 0 RON. These very low ONs limit the amounts that can be blended in gasoline to cost-effectively attain the 91−96 RONs of finished gasoline sold in the US. Furthermore, *n*-pentane has a low boiling point (36 °C), strongly impacting the dry vapor pressure equivalent (DVPE) of finished gasoline. DVPE is regulated by the Environmental Protection Agency (EPA), thus limiting the amounts of pentane that can be blended. Conversely, the oxygenated pentane analogues tested in this study have much higher ONs and boiling points, giving them a higher potential for blending with gasoline than pentane.

Table 2. Low-Net-Carbon Oxygenate Fuels Selected for Study

oxygenate	ethanol	methyl-pentanoate	1-pentanol	2-pentanol
abbreviation	"ET"	"MP"	"P1"	"P2"
CAS number	64-17-5	624-24-8	71-41-0	6032-29-7
boiling point [°C]	78	126	138	119
density@15°C [kg/L]	0.789	0.885	0.815	0.805
oxygen [wt %]	34.8	27.6	18.2	18.2
LHV [MJ/L]	21.2	25.0	28.3	27.8
heat of vaporization (HOV)@25° C [kJ/kg]	919	380	509	608
RON	109	103	82	99
MON	90	101	76	91
octane sensitivity	19	2	6	8

This study explores the impacts of oxygenate chemistry on ϕ-sensitivity by investigating five-carbon oxygenate analogues of *n*-pentane, including methyl pentanoate, 1-pentanol, and 2-pentanol.

The final blends used in the engine experiments and computational fluid dynamics (CFD) simulations are detailed in Table 3. These blends are named following the pattern of "XX_##_YY", where "XX" is the abbreviation of the oxygenate (from Table 2), "##" is the volume % of this oxygenate in the blend, and "YY" is the abbreviation of the BOB (from Table 1), which makes up the balance of the blend. For example, "ET_10_87" consists of ethanol blended at 10% by volume into the RD-587 BOB, representing commercially available gasoline. ET_10_2B is the pure component surrogate of ET_10_87, which was used for CFD simulations in which a detailed chemical representation of distillate gasoline was infeasible. This ET_10_2B fuel was used as the "baseline" fuel for this study. The other three fuels are designed to match the reactivity of the baseline fuel (in terms of RON) as closely as possible while differing in ϕ-sensitivity.

Engine Setup. The engine selected for this study is detailed in Table 4 and Figure 2. Although this is a MD engine and slightly smaller in terms of cylinder size than most HD vehicles that ACI is targeted for, this was a compromise made to reduce the amounts of fuel needed for extensive testing and to leverage existing hardware. This engine is a modified version of the Ford power stroke V8 engine (a.k.a. the "Scorpion" engine), using the production piston, cylinder sleeve, connecting rod, intake and exhaust ports, valves, cam lift profiles, and fuel rail. The cylinder head, containing the intake and exhaust port structures, was based on the production head but modified for a single-cylinder engine block designed and built by Southwest Research Institute. This setup combines the optimized geometry of a production engine model with the reduced fuel consumption and support equipment requirements of a single-cylinder engine (vs the production of 8-cylinder engine).

This system is mostly unmodified from the same system used with conventional MCCI and diesel fuel that is further detailed in a previous study,[10] but three modifications were made since this previous study. The first modification was the addition of a charge air cooler to the intake, which was added to achieve low intake temperatures at high exhaust gas recirculation (EGR) rates to increase ACI load limits. The second modification was the use of a national instruments direct control

https://doi.org/10.1021/acs.energyfuels.3c01537
Energy Fuels 2023, 37, 12243−12258

Table 3. Fuel Blends and Key Properties

blend name	ET_10_87	ET_10_2B	MP_35_2B	P1_30_2C	P2_30_2B
oxygenate and target level [vol %]	ethanol 10%	ethanol 10%	methyl-pentanoate 35%	1-pentanol 30%	2-pentanol 30%
BOB	RD-587 BOB	BOB-2B	BOB-2B	BOB-2C	BOB-2B
oxygenate [vol %]	11.57	9.70	34.94	29.93	29.80
oxygenate [mol %]	23.11	21.13	37.47	36.67	36.26
carbon [wt %]	82.19	82.77	77.36	81.26	81.21
hydrogen [wt %]	13.57	13.57	11.78	12.93	13.00
oxygen [wt %]	4.24	3.65	10.86	5.81	5.79
density@15°C [kg/L]	0.751	0.756	0.800	0.772	0.767
LHV [MJ/kg]	41.69	41.50	37.56	40.36	40.63
HOV@25°C [kJ/kg]	425	407	348	413	412
RON[a]	90	92	91	91	91

[a]RON was measured with the advanced fuel ignition delay analyzer using a rapid measurement method.[25]

Table 4. Engine Specifications

base engine architecture	ford power stroke 6.7 L scorpion (MY2017)
displacement volume	0.83 L (single cylinder)
bore × stroke	99 × 108 mm
compression ratio	16.2:1
connecting rod length	177 mm
coolant inlet temperature	90 °C
oil temperature	90 °C
fuel injector model	Bosch CRI3-20 (Piezo)
injection orifice size	0.138 mm
injector umbrella angle	production: 150°; modified: 90°
injector # of holes	production: 8; modified: 6
cylinder pressure transducer	Kistler 6058A
charge amplifier	Kistler 5010
CA encoder	BEI 3600 count (0.1°res)

module used to send complex injection schedules to the injector (up to 16 per cycle).

The third and final change to the system was a modification of the fuel injector. The production injector was designed to inject fuel in a spray pattern optimal for MCCI but poorly designed for ACI, as shown in Figure 3. The "umbrella" angle of the production injector, i.e., the included angle between fuel jets in the same vertical plane, is too wide at 150°. This is ideal for conventional MCCI, in which highly retarded injection timings are used (usually later than −20°aTDC). However, using this angle at timings more advanced than −40°aTDC points the fuel spray directly at the cylinder wall and mixes liquid fuel with the oil film on the wall, a phenomenon known as "wall wetting". The lift of the intake valve also interferes with injection during most of the intake stroke, which is proposed in some ACI modes.

To address these concerns, a modified injector was produced with a reduced umbrella angle of 90°. This angle was selected as the narrowest angle that could be feasibly achieved through modification of the production injector tip. Although there are specially designed gasoline direct injection systems that can achieve a narrower spray cone, these would require extensive modification of the engine's cylinder head. The 90° angle is sufficient to keep the fuel spray clear of the intake valve and avoid wall wetting over a wide range of CAs. One concern with reducing the umbrella angle is that the reduced distance between individual jets could cause unwanted cross-jet interactions. Therefore, the number of jets was reduced from 8 to 6, with the 6-hole design found to produce optimal spacing between jets in preliminary CFD studies. To achieve the redesigned spray pattern, the original holes on a production injector tip were laser welded shut, and the new holes were machined via electrical discharge machining.

Determining Test Conditions. Preliminary tests with the modified injector made it clear that a strategy with fewer injections produced more consistent performance over time, and no more than three injections were desirable to maintain the coefficient of variation (CoV) of the indicated mean effective pressure (IMEP) within the

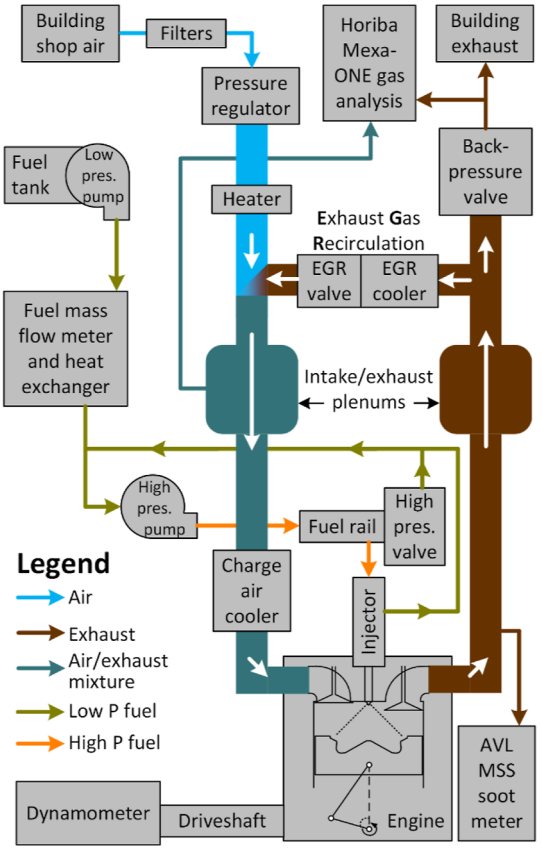

Figure 2. Test setup diagram.

stability limit over long periods of time. However, it was still necessary to design a strategy to determine the injection duration that would inject a certain amount of fuel. Previous work has indicated that it is ideal to have a late injection with approximately 20% of the total fuel,[21] so a schedule was designed to determine the duration needed to produce an injection with 20% of the fuel. This schedule (top of Figure 4) used five injections spaced far apart to prevent close-coupled injections from creating an inequal distribution of fuel between injections.

Once the injection duration needed to inject 20% of the total fuel was determined, the ϕ-sensitivity testing schedule (bottom of Figure 4) was employed. In this schedule, either two or three injections is used depending on the engine load. At lighter loads, two injections are used. The first injection starts at SOI_{early} and contains 80% of the fuel, which is intended to achieve a homogeneous distribution throughout the cylinder by the time of ignition. The second injection starts at SOI_{late} and contains 20% of the fuel, which is intended to produce a ϕ gradient

https://doi.org/10.1021/acs.energyfuels.3c01537
Energy Fuels 2023, 37, 12243−12258

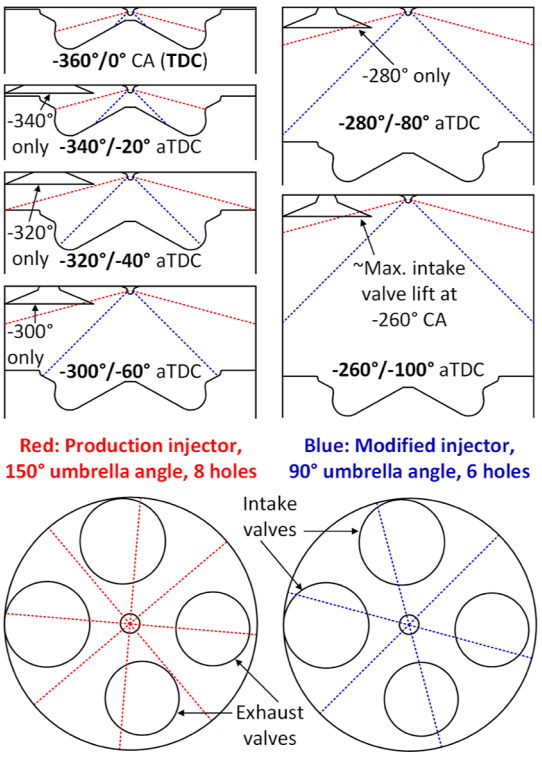

Figure 3. Fuel spray patterns produced by the original (red) and modified (blue) injectors. The top portion of the figure shows a sequence of side-on views of the cylinder and how the center line of each fuel jet aligns with the piston (and intake valve during the intake stroke). The bottom portion shows bottom-up views of the cylinder, showing the individual fuel jets in relation to the valves.

at the time of ignition. The steepness of the ϕ gradient, and thus the ignition timing, can be varied by varying SOI_{late}. At higher loads, to promote a more even distribution of fuel throughout the cylinder, a third injection is added, which starts at SOI_{mid}. This injection contains 20% of the total fuel, reducing the first injection to 60% of the fuel.

To compare ϕ-sensitivity at conditions most relevant to overall engine performance, this study is based on three "center point" test conditions. These three points cover a wide range of the engine's MCCI operating envelope. These points are the centers of start-of-injection (SOI) and EGR sweeps that will be performed to evaluate ϕ-sensitivity. The center points are based off an operating map provided by the engine's manufacturer but modified to bring ACI operation within certain limits with all the fuels tested. These limits are as follows:

- A knock limit of ringing intensity (RI) less than 5 MW/m^2.
- A stability limit of CoV of gross $IMEP_G$ less than 5%—i.e., a standard deviation of $IMEP_G$ < 5% of the mean.

Each of the center points is given a short name for easy reference in the form of one letter and two numbers, with the letter representing relative engine speed and the numbers representing roughly the percentage of full engine load.

Defining ϕ-Sensitivity Metrics. Engine ϕ-sensitivity analysis is based on heat release rate (HRR) analysis, which can identify the apparent timing of ignition. There are many valid methods of assigning an ignition point to the continuous HRR curve, as detailed and discussed in a previous study on this same engine.[26] The method used here is a variation of a method developed by Ortiz-Soto et al.,[27] which calculates the curvature κ of normalized HRR (HRR_{nor})

$$\kappa = \frac{\frac{d^2(HRR_{nor})}{dCA^2}}{\left(1 + \frac{d(HRR_{nor})}{dCA}^2\right)^{3/2}} \quad (2)$$

Ortiz-Soto et al. defined an ignition point at the average crank angle (CA) of two points: the peak of curvature and the peak of the 2nd derivative $d^2(HRR_{nor})/dCA^2$. For this study, the ignition point ("$HTHR_{start}$") is the CA at the peak of curvature only (disregarding the peak of the 2nd derivative). In the upper portion of Figure 5, $HTHR_{start}$ is shown to consistently track with a sharp transition point in the HRR, marking the transition between ITHR and high-temperature heat release (HTHR).

As SOI_{late} is retarded, the ϕ distribution becomes more and more stratified at the time of ignition, and $HTHR_{start}$ advances. The advance of $HTHR_{start}$ between two certain SOIs should be greater for more ϕ-sensitive fuels. This will form the basis of what is herein called "Type 1" ϕ-sensitivity analysis and has previously been proposed by Pintor et al.[28] These previous authors used another ignition point definition: CA_{10}, i.e., the CA where 10% of the total integrated heat release is reached. Pintor et al. measured the change of ignition timing (via CA_{10}) between two specific values of SOI_{late}. This study, to allow for flexibility in the SOIs used, measures the slope of ignition timing (via $HTHR_{start}$) with respect to SOI_{late} using the following equation

$$\frac{\Delta HTHR_{start}}{\Delta SOI_{late}} = \frac{HTHR_{start_a} - HRHR_{start_b}}{SOI_{late_b} - SOI_{late_a}} \quad (3)$$

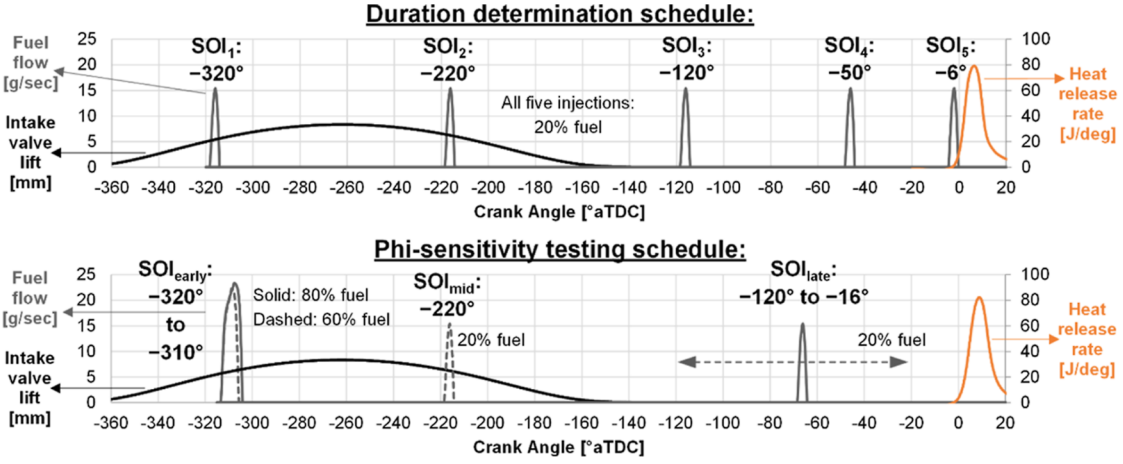

Figure 4. Specific ACI injection strategies used in this study. Fuel flow was modeled using the manufacturer's fuel flow data and measurements from an outside contractor that modified the injector for the ACI configuration. The bottom schedule is used for ϕ-sensitivity testing and will produce all the data in the Results section.

https://doi.org/10.1021/acs.energyfuels.3c01537
Energy Fuels 2023, 37, 12243−12258

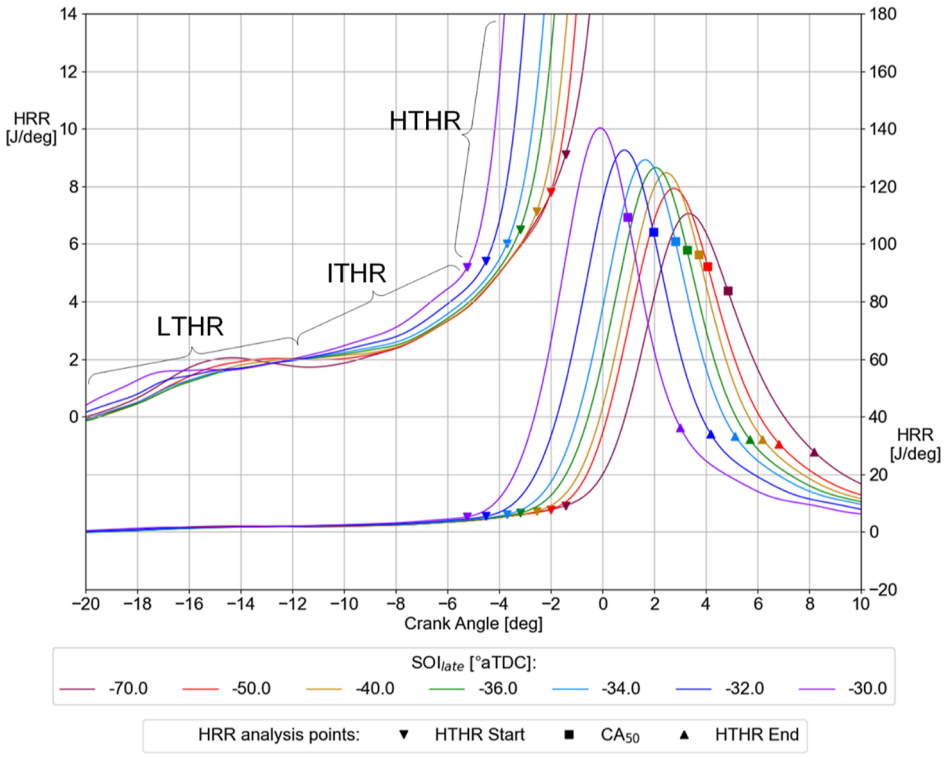

Figure 5. HRR analysis example: D25 condition, P1_30_2C fuel, SOI_{late} sweep.

In the above equation, a is a relatively advanced SOI_{late} and b is a relatively retarded one. For this study, the two CAs selected for SOI_{late}, a and b, were −50 and −36°aTDC, respectively, for reasons that will be illustrated in the Results section. However, these values are not meant to be universal and were chosen to evaluate the most ϕ-sensitive SOI_{late} region for this particular engine, injector, and set of fuels and test conditions. Much different values of a and b may be appropriate for different studies.

Another point of HRR analysis seen in Figure 5 is CA_{50}, which is used in another type of ϕ-sensitivity analysis that is called "Type 2" analysis in this study. Also, as previously devised by Pintor et al.,[28] this analysis finds the CA_{50} at which a RI limit is reached. Unlike Type 1 analysis, which must inherently involve a sweep of SOI_{late}, Type 2 analysis can be done with sweeps of other parameters as well, e.g., EGR sweeps in this study. Pintor et al. used the knock limit of 5 MW/m^2 as their RI limit for analysis, but this limit can be set to another value if a sweep in a certain condition does not produce knocking with all fuels.

The basis for the Type 2 ϕ-sensitivity analysis can be explained by another HRR analysis point, as shown in Figure 5, $HTHR_{end}$, which is defined as the point where HRR falls below 25% of its peak value. This produces a measurement of $HTHR_{duration}$ by taking the difference in CA between $HTHR_{end}$ and $HTHR_{start}$. Increased ϕ-sensitivity will widen this HRR peak by lengthening the sequential autoignition process—the differences in ignition delay between regions of different ϕ will be magnified. This is one of the benefits of ϕ-sensitive fuels in ACI: by widening the HRR peak, the MPRR will also be lower. This should allow more ϕ-sensitive fuels to reach more advanced CA_{50} before reaching the knock limit.

To summarize:

- Type 1 ϕ-sensitivity analysis: $\Delta HTHR_{start}/\Delta SOI_{late}$ (ignition delay).
- Type 2 ϕ-sensitivity analysis: CA_{50}@RI limit (rate of sequential autoignition).

In evaluating both metrics, great care must be taken to ensure that only one test condition changes along a sweep and all other test conditions are held constant, both along the sweeps and between fuels, to maintain an "apples-to-apples" comparison. Of course, some inherent differences between fuels and test conditions are unavoidable, especially when compared to more tightly controlled bench experiments, so these metrics cannot be taken as perfect indicators of ϕ-sensitivity.

Peak Load Testing. A final set of tests was conducted with each fuel after the ϕ-sensitivity analysis: peak load testing. The end goal of finding ϕ-sensitive fuels is to increase the peak load at which a given engine can operate with ACI alone, so higher ϕ-sensitivity should lead to a higher peak load if all else is held the same. For these tests, all conditions from Table 5 are held the same except:

Table 5. Center Point Test Conditions Derived from Manufacturer's Test Conditions

center point	B20	D25	F35
speed [RPM]	1000	1300	1600
$IMEP_G$ [bar]	3.0	4.2	6.0
fuel pump inlet temp. [°C]	40	40	40
rail pressure [bar]	400	400	400
intake temperature [°C]	58	48	48
intake pressure [bar abs]	1.3	1.5	1.7
exhaust pressure [bar abs]	1.7	2.0	2.3
global ϕ [-]	0.31	0.38	0.56
approx. EGR [vol %]	20%	30%	40%
SOI_{early} [°aTDC]	−310°	−315°	−315°
SOI_{mid} [°aTDC]	N/A	N/A	−220°
SOI_{late} [°aTDC]	−28°	−50°	−70°

- SOI_{late} is advanced to −120°aTDC, creating a relatively homogeneous charge and retarding combustion to reduce knock.
- The duration of SOI_{early} is increased until the knock limit is approached.
- EGR is increased until the stability limit is approached.

These last two changes are implemented in an iterative process starting from the "center point" condition. The peak load is achieved

https://doi.org/10.1021/acs.energyfuels.3c01537
Energy Fuels 2023, 37, 12243−12258

when the knock and stability limits converge, i.e., neither SOI_{early} duration nor EGR can be increased without going over one of the limits.

CFD Modeling. The CFD simulations were conducted to match the engine conditions from Table 5 using only a select few points on the SOI sweeps. The purposes of these simulations were to determine the ϕ distributions produced with various SOI_{late} timings and to gain insight on the appropriate windows of SOI_{late} to use for ϕ-sensitivity testing and ACI. CONVERGE CFD software[29] was used to perform the CFD simulations. The boundaries of the simulation were set at cross-sectional planes set several diameters upstream and downstream of the intake and exhaust valves, respectively, as shown in Figure 6. The

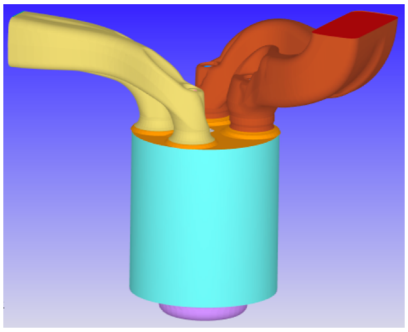

Figure 6. 3D Geometry (ports, cylinder, piston, and injector) used for the CFD simulation.

conservation equations are solved with a finite volume method using second-order spatial discretization with implicit first-order time accuracy. The liquid spray and gas phase interactions are solved in the Lagrangian−Eulerian method. The droplets breakup, collision, and evaporation are modeled as well. We used the renormalized group k-epsilon model for the turbulence modeling. The computational grid shown in Figure 7 is automatically generated in Converge using the cut-

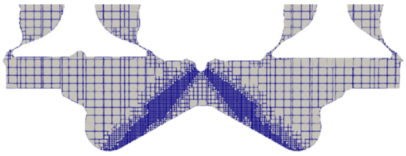

Figure 7. Computational mesh inside the cylinder showing the 3 levels of fixed embedding refinement near the injector and the 3 levels of AMR for the spray flow outside the fixed embedding.

cell Cartesian method. The initial base grid used for the single-cylinder engine was 2 mm. To increase the accuracy of spray injection and droplets evaporation/mixing, we used three levels of fixed embedding refinement for each of the 6 injector nozzles as well as three levels of adaptive mesh refinement based on the velocity and temperature gradients, which translated to the minimum grid size of 0.25 mm at the most critical regions. The total computational mesh was limited to a maximum of 2,000,000 cells to avoid significantly higher computational costs. The liquid thermo-physical properties of each component from the surrogate mixture were obtained from the NIST database.[30] A more detailed description of the computational method can be found in our previous study.[31]

RESULTS

The results are divided into three sections:

1. Engine/CFD SOI sweeps, in which ϕ-sensitivity is evaluated with the "Type 1" metric.
2. Engine EGR sweeps, in which ϕ-sensitivity is evaluated with the "Type 2" metric.
3. Engine peak load tests, in which the effect of ϕ-sensitivity of peak load is evaluated, and the overall emissions are compared with environmental limits for conventional diesel combustion.

SOI Sweeps. Figure 8 shows the shifts in combustion phasing for all fuel blends tested as SOI_{late} is shifted, for each of the three test conditions detailed in Table 5. The ET_10_87 fuel had a much different behavior than the other fuels, indicating that surrogate BOB-2B does not provide a perfect representation of the full boiling range gasoline RD-587 BOB's ACI behavior. The analysis of this study will focus on the other, pure component BOB fuels, whose phasing was much more closely aligned with each other than ET_10_87.

The range of SOI_{late} that is most pertinent to ϕ-sensitivity analysis in this study is approximately −50 to −36°aTDC. This is the window that all the fuels could cover in all three test conditions, well within the knock and stability limits. Within this window, SOI_{late} could be retarded, advancing both $HTHR_{start}$ and $CA_{50,}$ without decreasing HTHR duration significantly. Advancing SOI_{late} to earlier timings produced increases in duration, cycle-to-cycle variability (see Supporting Information), and unburnt hydrocarbons (UHC, see Supporting Information), indicating wall wetting. Conversely, retarding SOI_{late} to later timings produced decreases in duration with sharp increases in NO_X and soot emissions, indicating a shift toward mixing-controlled combustion. For these reasons, this window of approximately −50 to −36°aTDC was selected as the range of SOI_{late} to conduct the "Type 1" ϕ-sensitivity analysis.

To confirm the appropriateness of this SOI_{late} window, CFD simulations of the ET_10_2B fuel were conducted to demonstrate the change in the ϕ distribution at the time of ignition between the two ends of the window, as shown in Figure 9. Figure 9 shows the differences in the ϕ distribution throughout the combustion chamber at the point of ignition for different points on the B20 SOI sweep. At the start of the ϕ-sensitivity evaluation window (SOI_{late} = −50°aTDC), most of the fuel is concentrated between a ϕ of 0.1 and 0.3 when the charge ignites. At the end of the ϕ-sensitivity evaluation window (SOI_{late} = −36°aTDC), there is an increase in the amount of fuel contained in zones of a phi between 0.3 and 0.8 and thus an increase in stratification.

The comparative cross-sectional images in Figure 10 show how the SOI_{late} range is dependent on the injector/piston combination used in this study, and other ranges will be appropriate for other studies. For the SOI = −50° case (left column), the piston has ascended just enough that the late injection is contained within the bowl, as shown in the CAD = −44 row. In the SOI = −36° case (middle column), the piston bowl shape is such that the distance at which the fuel jet impinges on the piston bowl (as shown in the CAD = −30 row) is relatively unchanged relative to the SOI = −50° case. However, in the SOI = −28° case (right column), the piston starts to impinge much closer to the injector (CAD = −22 row), giving the fuel less distance to mix and evaporate, whereas this impinging distance was relatively constant (and longer) for the SOI_{late} window of −50° to −36°.

Although later SOI_{late} timings could produce even more stratifications, a SOI_{late} of −28°aTDC was the latest to contain no rich zones (ϕ > 1) remaining in the mixture at the observed ignition timing from the experiments. A SOI_{late} of −24°aTDC still contained rich zones at the point of ignition, indicating a transition from ACI to MCCI, which is backed up in the experiments by a simultaneous reversal in the $HTHR_{start}$ trend, seen in Figure 8.

https://doi.org/10.1021/acs.energyfuels.3c01537
Energy Fuels 2023, 37, 12243−12258

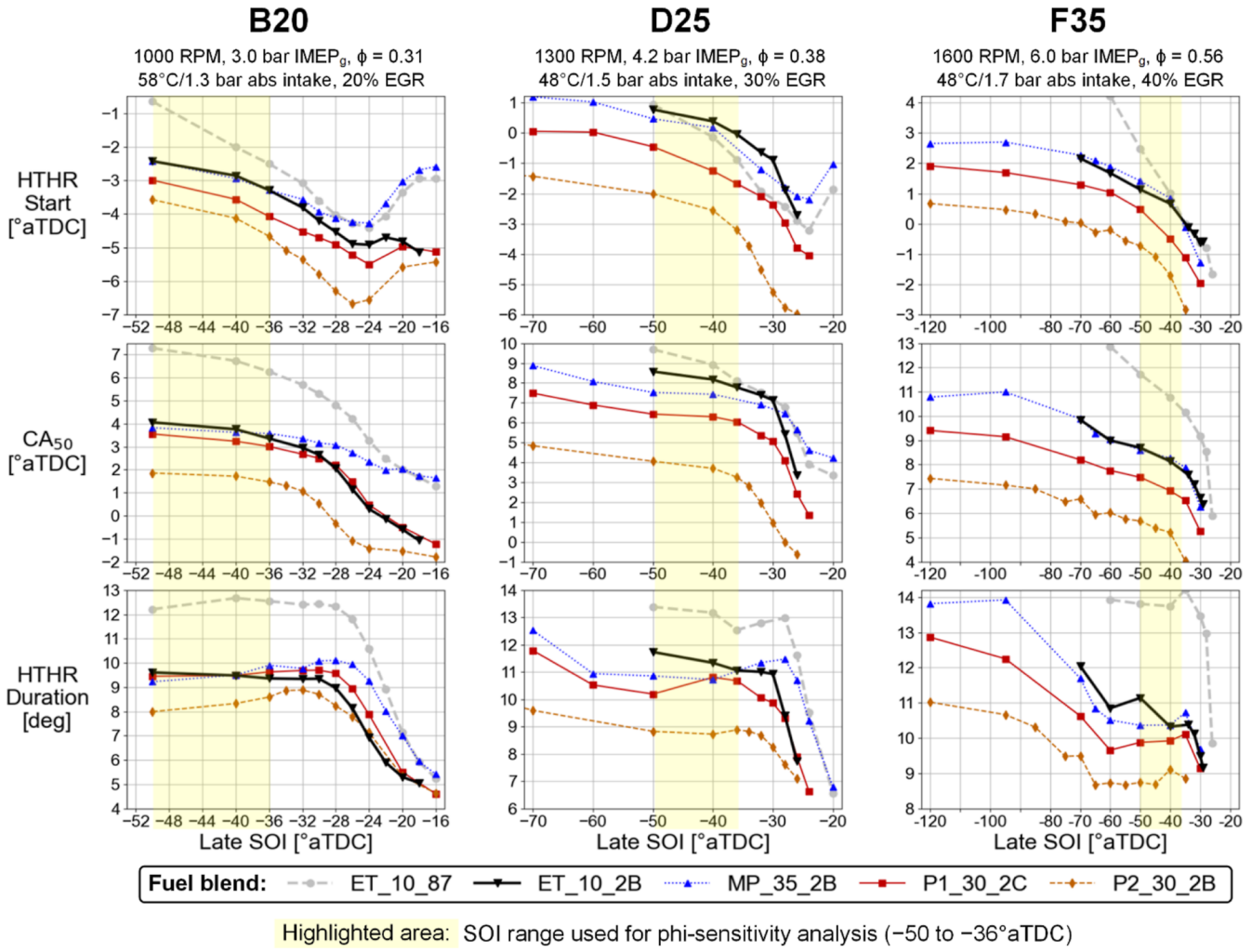

Figure 8. Combustion phasing over the SOI_{late} sweeps.

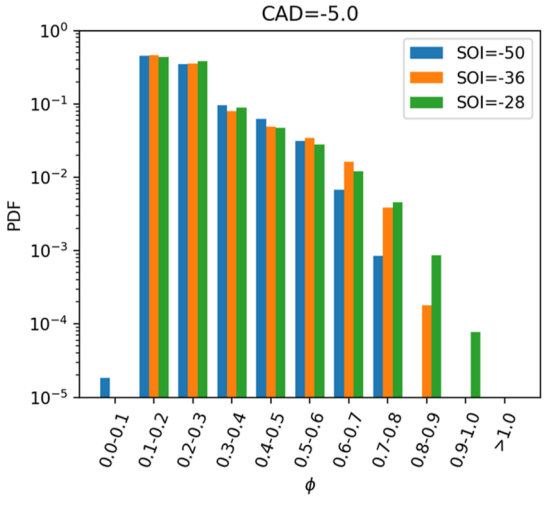

Figure 9. CFD-simulated ϕ distributions in terms of mass fraction for the B20 test condition with the baseline ET_10_2B fuel.

For the ϕ-sensitivity analysis, it was determined that the "Type 1" analysis was the only type appropriate for the SOI_{late} sweeps, since using the "Type 2" analysis would require using SOIs retarded into the range of about −20°aTDC, where some mixing-controlled combustion is being produced. The results of the Type 1 analysis are given in Figure 11, showing that all 3 of the C_5 oxygenate blends increase ϕ-sensitivity, albeit methyl pentanoate less so than the pentanols. The higher the load, the greater the differentiation in ϕ-sensitivity between the fuels.

EGR Sweeps. Full EGR sweep data can be found in the Supporting Information, while Figure 12 shows two key trends related to ϕ-sensitivity: HTHR duration and RI, which are almost perfectly inverse of each other with respect to CA_{50}. This is expected since a longer HTHR duration will reduce pressure rise rates and thus RI. The difference in the ϕ-sensitivity of these fuels is readily apparent in these plots, as lines shifted further to the left indicate more ϕ-sensitive fuels with more a staggered sequential autoignition process during ACI.

The Type 2 ϕ-sensitivity analysis of the EGR sweeps, shown in Figure 13, agrees well with the Type 1 analysis of the SOI sweeps from Figure 11. Once again, there is little to no increase in ϕ-sensitivity in the methyl pentanoate blend relative to the ethanol blend but a significant increase in ϕ-sensitivity in the pentanols.

The differences in the ϕ-sensitivity can be illustrated by the HRR traces in Figure 14. These traces use a different point on the EGR sweep for each fuel, but the same SOI_{late}, giving them a similar phi distribution despite differences in the global ϕ. The baseline fuel, methyl pentanoate blend, and 2-pentanol blend have very well-synchronized $HTHR_{start}$, but the more ϕ-

https://doi.org/10.1021/acs.energyfuels.3c01537
Energy Fuels 2023, 37, 12243−12258

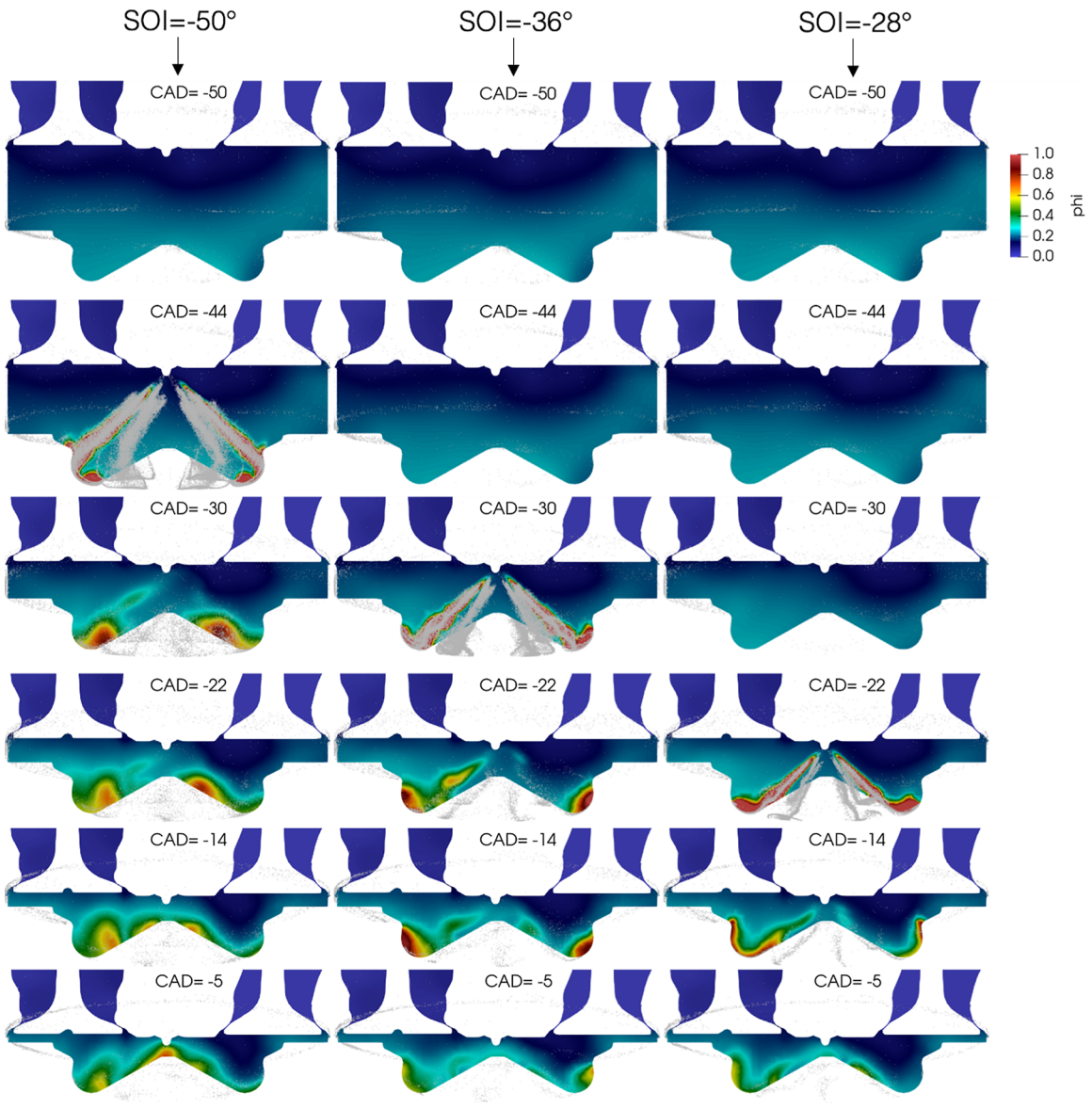

Figure 10. 2D contour figures of the equivalence ratio inside the cylinder during the second injection for the B20 case with the three different SOI cases. The gray particles show the spray still in the liquid phase.

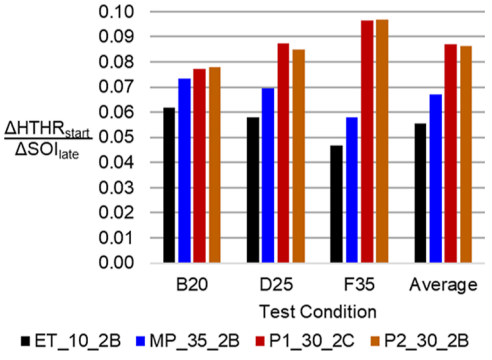

Figure 11. ϕ-sensitivity of fuel blends measured with Type 1 analysis over SOI_{late} sweeps from −50 to −36°aTDC.

sensitive fuels have lower HRR at the peak and higher HRR toward the end of combustion, leading to a later HRR_{end} (and thus a longer combustion duration). Although a well-synchronized point was not found on the sweep of the 1-pentanol blend, its increased ϕ-sensitivity is still apparent: although the 1-pentanol blend HRR is advanced compared to the baseline, it still has a lower peak and the same duration.

Looking further back in the HRR, and fixing the global ϕ to be constant, differences in the LTHR and ITHR phases become apparent between fuels, as shown in Figure 15. Each of the C_5 oxygenate blends creates a significant increase in the amount of LTHR and advances ITHR relative to the baseline. However, the largest increase in LTHR occurred with the methyl pentanoate blend, which did not experience a significant increase in ϕ-sensitivity. This indicates that increased LTHR/ITHR do not necessarily correspond with ϕ-sensitivity when comparing different fuels.

Peak Load. The peak loads found in Figure 16 mostly agree with the ϕ-sensitivity testing, with one main exception: at the 1600 RPM condition (based off F35), the baseline fuel was found to have the highest load limit, despite having the lowest ϕ-sensitivity according to the other indicators. Despite this anomalous result, the 1-pentanol blend produced an average

https://doi.org/10.1021/acs.energyfuels.3c01537
Energy Fuels 2023, 37, 12243−12258

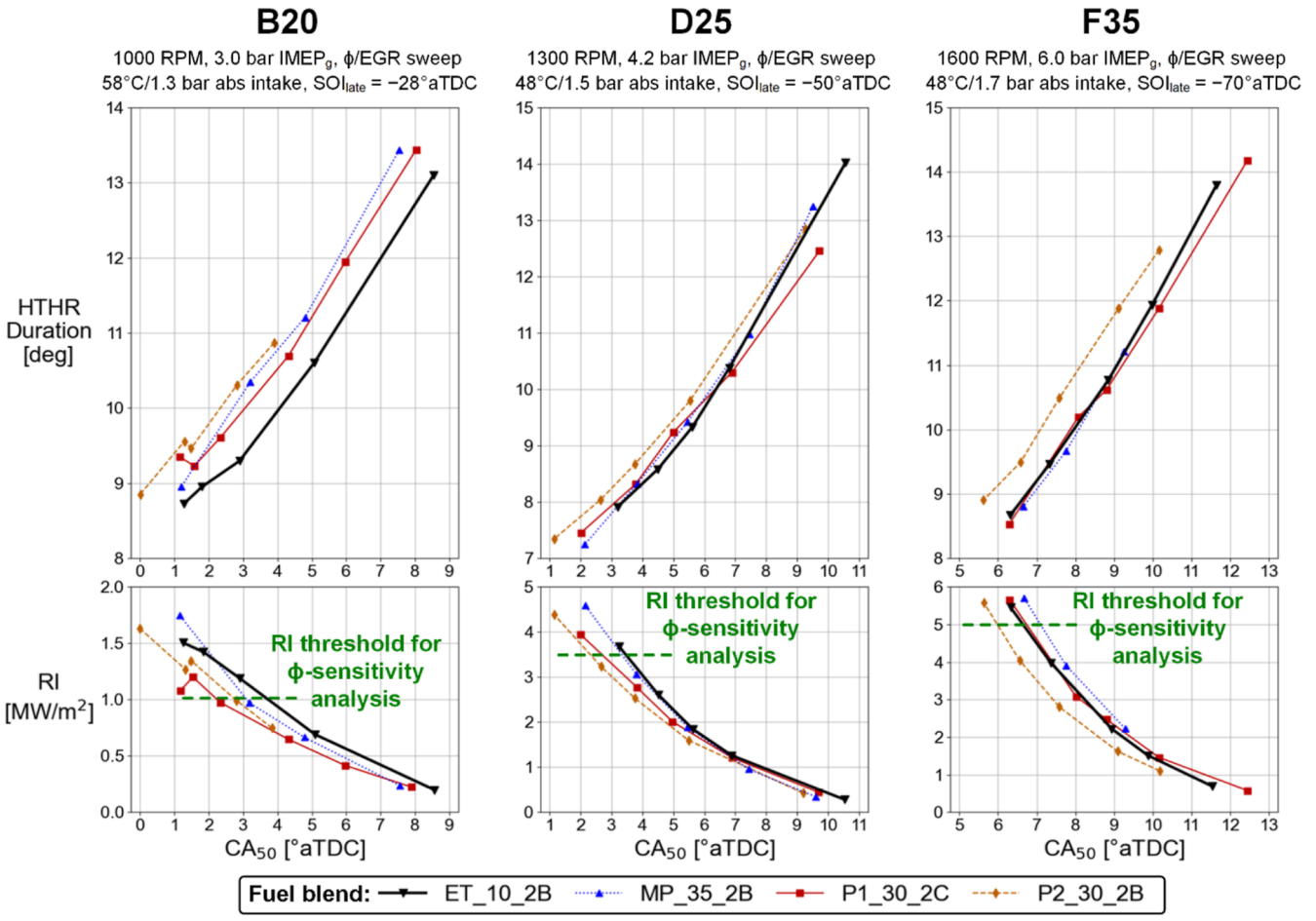

Figure 12. HTHR duration and RI vs CA_{50} for EGR sweeps. Green dashed lines indicate the RI thresholds used for Type 2 ϕ-sensitivity analysis. High ϕ-sensitivity fuels allow for more advancement of CA_{50} before the RI limit is reached by extending the combustion duration.

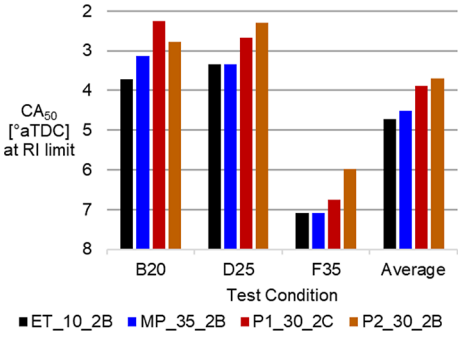

Figure 13. ϕ-sensitivity of fuel blends measured with Type 2 analysis over all EGR sweeps.

increase of 57 kPa in the peak IMEP vs the baseline fuel, with the largest increase of 108 kPa occurring in the 1000 RPM condition (based off B20).

Although increases in peak load are a primary goal of increased ϕ-sensitivity, further effects of the increased ϕ-sensitivity in these tests can be seen in Figure 17, which shows several emissions and efficiency parameters from these peak load tests. The 1600 RPM ACI tests are also compared to conventional MCCI tests with ultra-low sulfur diesel (ULSD) at a similar test condition, which gives an indication of how ACI performance compares with the MCCI performance that it aims to replace. The emissions plots show emissions limits from the California Air Resources Board (CARB) that will be phased in by 2031.[32] While these CARB limits are intended to be evaluated over an entire dynamometer test cycle rather than a steady-state test condition, they still provide a suitable yardstick for whether ACI has the potential to eliminate the requirement for aftertreatment.

The ϕ-sensitivity of the fuel does not appear to have an effect on NO_X or soot emissions based on the lack of correlation in both Figure 17 and other emissions trends shown in the Supporting Information. Soot emissions were all an order of magnitude below the CARB limit, which is itself an order of magnitude below the engine-out emissions from ULSD. This strongly indicates that ACI can eliminate the need for soot aftertreatment systems such as DPF. Although total PM may contain organics other than soot that is not measured here, it seems plausible that an oxidation catalyst may suffice to control them. NO_X emissions were all below the Federal test procedure limit, but not all were below the low load cycle (LLC) limits set for low speed/load conditions in slow urban traffic, where NO_X emissions are of most concern. This indicates that at least some aftertreatment of NO_X may be necessary for ACI engines in the strictest regulatory environments. This is especially true given the relatively high NO_2/NO ratio in ACI (>0.2) relative to MCCI (<0.05) and the greater environmental harm caused by NO_2.

The ϕ-sensitivity of the fuel does appear to have some effect on the combustion efficiency (CE) of ACI, with the two ϕ-

https://doi.org/10.1021/acs.energyfuels.3c01537
Energy Fuels 2023, 37, 12243−12258

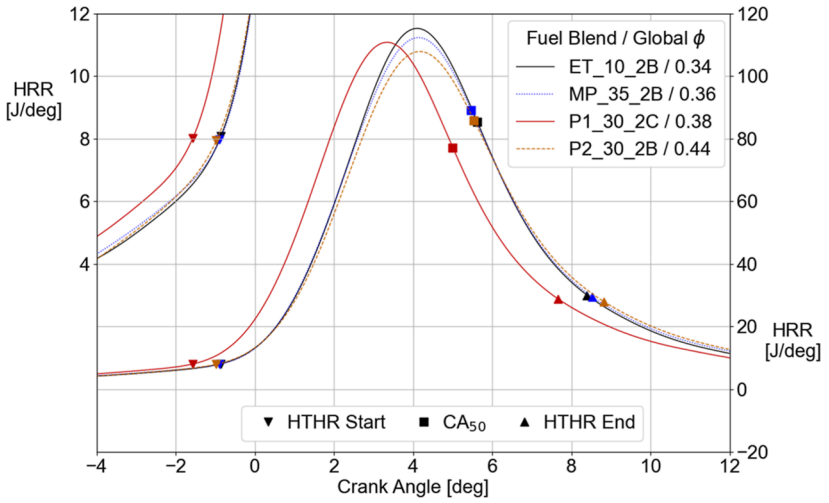

Figure 14. Selected HRR traces from the D40 EGR sweeps. These selected traces demonstrate the effect of increased ϕ-sensitivity on the HRR. Compared to the baseline, 1-pentanol can be advanced with a lower peak HRR and the same duration (distance between HTHR start and end), meanwhile, 2-pentanol has a lower peak HRR and a longer duration at the same $HTHR_{start}$ timing as the baseline.

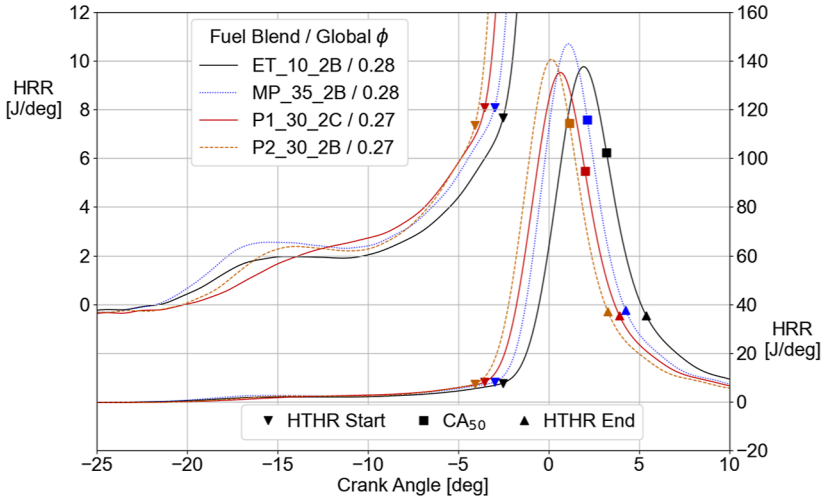

Figure 15. Selected HRR traces from the D40 EGR sweeps. These selected traces show the difference in LTHR and ITHR between fuels at the same global ϕ.

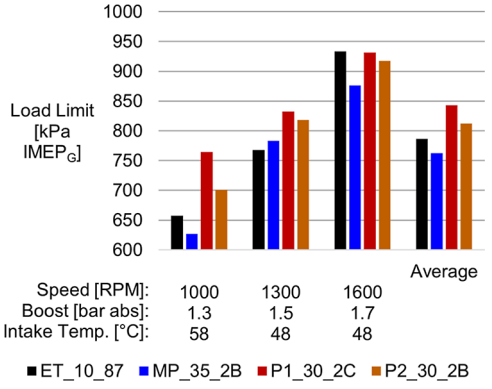

Figure 16. Differences in peak load across the fuels at three different test conditions.

sensitive pentanol blends increasing CE by about 0.5% over the baseline. Although the differences in CO and UHC emissions are not as apparent, this is due to the lower heating values of these fuels, which causes them to leave behind more unburnt emissions than the baseline fuel at the same CE. CO emissions are all less than half of the CARB limit, but UHC emissions are all well above it, and both are about an order of magnitude above the ULSD MCCI (which typically has CE well above 99%). This means that an oxidation catalyst for removing UHC emissions will be necessary for ACI operation, even with the most ϕ-sensitive fuels. Rather than using the original CARB limit for UHC, it is more useful to calculate the engine-out emissions that will produce tailpipe emissions below the limit after a catalytic converter (CAT) has removed most of the UHC. CAT efficiency typically starts at 99% with a new unit and degrades over its lifetime to around 95%, so a value of 97% CAT efficiency was used to calculate the upper UHC limit seen in Figure 17. The ϕ-sensitive pentanols appear to reduce UHC emissions below this limit, whereas baseline emissions are right at the limit. However, a key parameter that effects both CATs and NO_X aftertreatment systems is exhaust temperatures, which must generally be kept high to ensure catalyst performance but are generally lower in ACI than MCCI. The ϕ-sensitive fuels appear to increase exhaust temperature, especially in the lowest-load condition, which may be a result of the increased CE.

https://doi.org/10.1021/acs.energyfuels.3c01537
Energy Fuels 2023, 37, 12243−12258

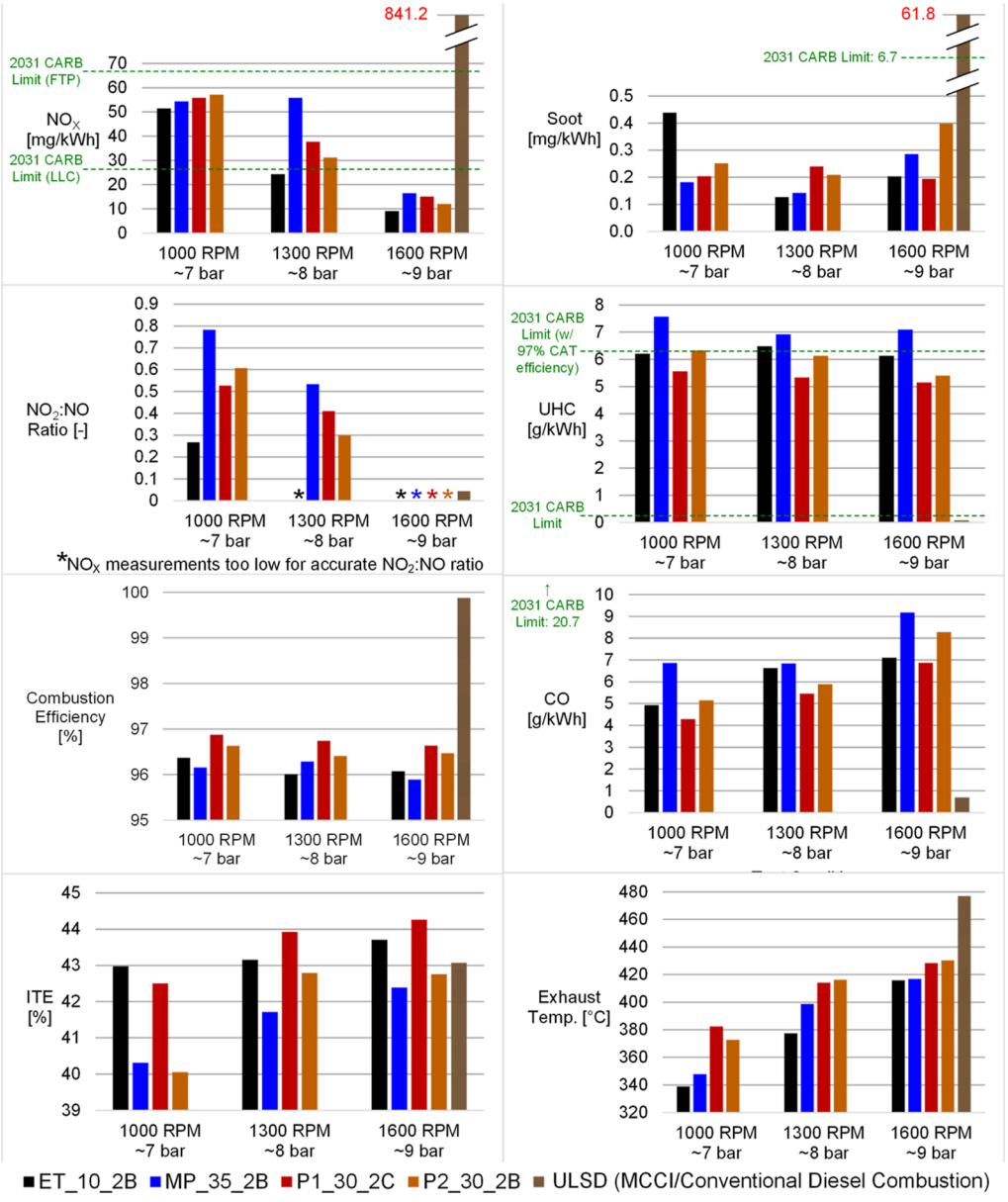

Figure 17. Emissions and efficiencies of the different fuels during peak load tests. Also shown in the 1600 RPM condition is an MCCI (conventional diesel combustion) condition using ULSD, which puts into perspective how these emissions compare to conventional CI engine emissions. The CARB limits to be phased in by 2031 are given for the emissions, including the level of engine-out UHC emissions that would produce the tailpipe limit with a CAT efficiency of 97%.

Determining the full effect of these altered exhaust temperatures on aftertreatment performance and compatibility would require a complex analysis of transient conditions beyond the scope of this study.

In terms of overall indicated thermal efficiency (ITE), the baseline and 1-pentanol fuels had greater ITE than MCCI, but the other oxygenate blends did not. These ITE differences are consistent in the other test conditions shown in the Supporting Information. It is unclear where these ITE differences emerge from, but it must be noted that the only oxygenate blend with higher ITE was the 1-pentanol blend, which used a different BOB than the other fuels. It is possible that the oxygenate blends tend to reduce ITE slightly due to their reduced heating values, but the 1-pentanol blend canceled out this effect by changing the BOB.

DISCUSSION

Without a direct comparison to another study, it is difficult to contextualize the magnitude of the ϕ-sensitivity benefits from the pentanol blends. One study that these results can be directly compared to is the work of Pintor et al.[28] at Sandia National Laboratories. The Sandia study compared the same baseline RD-587 fuel from our study with a hydrocarbon blend ("CB#1") designed to simultaneously maximize ϕ-sensitivity, RON, and octane sensitivity.[24] The Sandia study used the same ACI injection strategy as our study, but with a much higher level of intake air heating (160 °C) to allow a lower compression ratio (14:1) and a wider range of SOI_{late} than our study. The Sandia study also used a different piston and different injector with a much lower injection pressure (120 bar) and kept engine speed (1200 RPM) and global phi (0.36) constant while conducting

https://doi.org/10.1021/acs.energyfuels.3c01537
Energy Fuels 2023, 37, 12243−12258

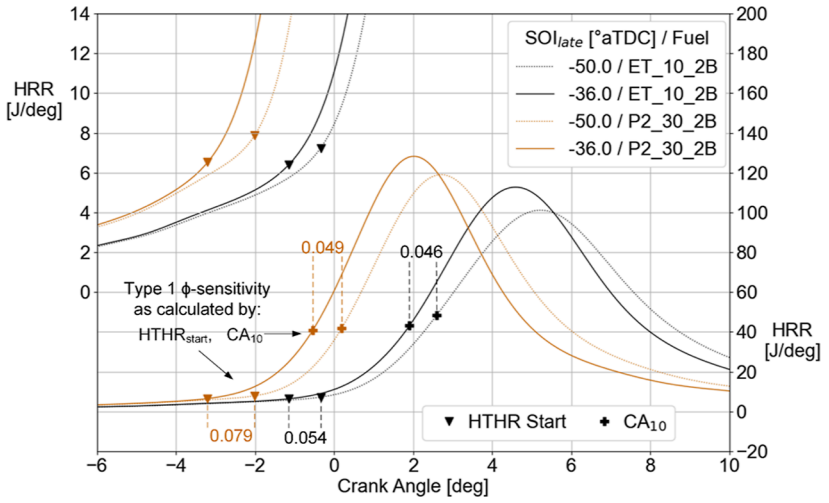

Figure 18. Calculation of Type 1 ϕ-sensitivity metric using HTHR$_{start}$ vs CA$_{10}$. Using CA$_{10}$ will make it seem as though there is no difference between these fuels, despite the fact that the ET_10_2B traces are clearly closer together than the P2_30_2B traces at the very start of HTHR (upper left). HTHR$_{start}$ is necessary to accurately capture the point of transition from ITHR to HTHR and calculate ϕ-sensitivity independently of combustion phasing.

SOI$_{late}$ sweeps at 3 different intake pressures: 1.0, 1.3, and 1.6 bar.

To apply the Type 1 ϕ-sensitivity metric to the Sandia results, detailed HRR data was not available, so CA$_{10}$ was used in place of HTHR$_{start}$. Only one of the three sweeps (the 1.0 bar intake pressure sweep) had the full CA$_{10}$ data reported, and the SOI$_{late}$ range had to be slightly altered to −50 to −35°aTDC (or 310 to 325° according to the Sandia convention) to calculate the ϕ-sensitivity. This gave the RD-587 fuel a Type 1 ϕ-sensitivity of 0.081 in the one Sandia condition for which it could be calculated. Making the same change from HTHR$_{start}$ to CA$_{10}$, our three test conditions gave the RD-587 fuel an average Type 1 ϕ-sensitivity of 0.105 (with a standard deviation of 0.040 across the three test conditions). This serves as a good "sanity check" that the two studies are producing similar results with the same fuel (0.081 in the Sandia study, 0.105 in our study), despite the different test conditions, including very different pistons, injectors, and injection pressures (120 bar at Sandia vs 400 bar in this study), which would cause large changes in the relation between SOI$_{late}$ and ϕ distribution.

What is most interesting to compare across studies are the fuel-dependent ϕ-sensitivity changes. In the Sandia study, Type 1 ϕ-sensitivity (with CA$_{10}$) increased from 0.081 to 0.107 (a 32% increase) when using their specially designed CB#1 hydrocarbon fuel. In this study, average Type 1 ϕ-sensitivity (with HTHR$_{start}$) increased from 0.056 with the baseline fuel to 0.067 with the methyl pentanoate blend (a 21% increase), 0.087 with the 1-pentanol blend (a 57% increase), and 0.086 with the 2-pentanol blend (a 56% increase). This does not necessarily mean that the pentanols caused a larger ϕ-sensitivity increase than the CB#1 blend, for the reasons stated below.

It may seem strange that CA$_{10}$ was not used to re-calculate our numbers for a more direct comparison with Sandia's numbers. The reason is that our data behave much differently when using CA$_{10}$ to calculate ϕ-sensitivity instead of HTHR$_{start}$—in fact, ϕ-sensitivity would appear to decrease with each of the oxygenate blends. However, this is not due to an actual decrease in ϕ-sensitivity but due to the shortcomings of defining CA$_{10}$ as the point of ignition, as illustrated by Figure 18. This shows the points used to calculate the Type 1 ϕ-sensitivity metric using both CA$_{10}$ and HTHR$_{start}$. The upper-left portion of Figure 18 zooms in on the transition between ITHR and HTHR and how HTHR$_{start}$ accurately captures this transition, as previously illustrated in Figure 5. The horizontal distance between these points matches the separation between the HRR traces immediately after HTHR begins. CA$_{10}$, however, occurs well after HTHR has progressed and, in the case of the ET_10_2B fuel especially, the HRR traces begin to diverge. As a result, the horizontal spacing between the CA$_{10}$ points (and thus the calculated ϕ-sensitivity) ends up about the same for the two fuels, despite there being clearly a smaller difference in the ignition timing of the ET_10_2B fuel than the P2_30_2B fuel. Accurately gauging ignition timing and thus ϕ-sensitivity may require more detailed HRR analysis methods than the simple CA$_{XX}$ methods, which show a tendency to drift up and down the HRR curve as SOI changes. These issues are discussed further in a previous analysis of conventional MCCI.[26]

For the above reasons, the type 2 ϕ-sensitivity metric makes a better link between the two studies. Both studies used the same CA$_{50}$ HRR evaluation, and it was reported for all 3 of Sandia's test conditions. Similar to our study, the change in CA$_{50}$ at the RI limit varied significantly between the three test conditions in the Sandia study, but the advance of CA$_{50}$ with the CB#1 test fuel was consistent enough to affirm the ϕ-sensitivity benefits. From the comparison in Table 6, it appears that the increased ϕ-sensitivity from the Sandia CB#1 fuel was about the same magnitude as the pentanol blends in our study. However, the same caveats as before still apply: the two studies used very different test conditions, pistons, injectors, and injection pressures.

Table 6. Changes in Type 2 ϕ-Sensitivity Metric between Baseline and Test Fuels, Our Study vs Sandia Study,[28] °aTDC, Averaged across 3 Test Conditions

study	our study			Sandia study
test fuel	MP_35_2B	P1_30_2C	P2_30_2B	CB#1
average change	0.20°	0.83°	1.03°	1.03°
std. dev	0.34°	0.58°	0.08°	0.51°

https://doi.org/10.1021/acs.energyfuels.3c01537
Energy Fuels 2023, 37, 12243−12258

Another major difference between our study and the previous Sandia study was the relative ignition timing of the fuels when SOI_{late} was highly advanced, and the ϕ distribution was very homogeneous. In the Sandia study, the test fuel was designed such that ignition was simultaneous with the baseline fuel with highly advanced SOI_{late}, and differences in the ϕ-sensitivity caused the timing of the two fuels to diverge as SOI_{late} was retarded. Thus, the ϕ-sensitivity metrics in the Sandia study were based on how the CA_{10} and CA_{50} changed from a common starting point. In our study, on the other hand, there was no common starting point. Our test fuels have different ignition timings from the baseline fuel and from each other when SOI_{late} was highly advanced, despite our best efforts to design the fuels to have reactivities as similar as possible. Synchronizing the starting points of each of the test fuels would have required a much more extensive, iterative fuel design and engine testing process, and we chose to spend our limited resources to do a thorough comparison of multiple fuels instead. The design of the engine ϕ-sensitivity metrics in this paper allows ϕ-sensitivity of several fuels to be compared even if the starting point of ignition is not perfectly synchronized, which is ideal for enabling the practical evaluation of as many fuels as possible.

The next step with this work is to link the ϕ-sensitivity metrics measured in engines to the ϕ-sensitivity metrics measured in benchtop experiments[33,34] and kinetics simulations.[24,33] All three forms of ϕ-sensitivity evaluation are needed to fully validate simulations of the benefits that ACI engines and ϕ-sensitive fuels can confer. Kinetic mechanisms for the pentanols are currently under development at Lawrence Livermore National Laboratory.[35]

CONCLUSIONS

Two oxygenated pentane substitutes, 1-pentanol and 2-pentanol, were found to increase the ϕ-sensitivity of gasoline in ACI engine combustion, while another, methyl pentanoate, was not. Two ϕ-sensitivity metrics were developed: the first ("Type 1") measured the sensitivity of ignition timing to the timing of the latest injection ("SOI_{late}") in a multi-injection ACI schedule. The second ("Type 2") measured the advance of CA_{50} before a RI limit of 5 MW/m̂2 was reached. When blended at 30% with a pure component hydrocarbon BOB, 1-pentanol and 2-pentanol increased Type 1 ϕ-sensitivity by 57 and 56%, respectively, while advancing the Type 2 knock limits by 0.83 and 1.03°, when compared to the baseline E10 gasoline with the same RON. For 1-pentanol, this translated to an increase in the load limit of ACI combustion of 57 kPa $IMEP_G$. These increases in ϕ-sensitivity did not lead to increases in ITE, although ACI combustion was still able to demonstrate improved ITE over conventional diesel combustion despite lower CE. The ϕ-sensitive pentanols yielded increased ACI CE and exhaust temperatures over the less ϕ-sensitive fuels, and engine-out CO, NO_X, and soot levels with all fuels were low enough to meet future emissions standards, at least in the steady-state conditions tested. The UHC emissions were, on average, at a level where a CAT would need to remove 97% of the emissions to meet the 2031 CARB standards, with the pentanol blends showing slightly lower UHC due to increased CE. CFD analysis was used to determine the relation of the ϕ distribution throughout the combustion chamber in relation to the SOI timing and which ranges of SOI were appropriate to use in calculating ϕ-sensitivity.

The primary result of this study was the finding of increased ϕ-sensitivity in the 1- and 2-pentanol blends, indicating that these fuels can be of interest both as low-carbon gasoline blendstocks and as fuels that will enable HD engines to operate in ACI modes, reducing NOx and PM emissions. A secondary outcome was the ϕ-sensitivity metrics developed in this paper, which can be applied to fuels that do not necessarily have the same ignition timing when the ϕ distribution is homogeneous, allowing many fuels to be tested in the same engine and same test conditions without extensive fuel design. However, further work must be done to connect these engine-based ϕ-sensitivity metrics with those developed for benchtop experiments and kinetic simulations. Ideally, future studies should include a first round of ϕ-sensitivity "screening" on larger numbers of fuel candidates using lab experiments and simulations and then a second round of confirmation testing on engines with a smaller, down-selected list of the most promising fuel candidates.

ASSOCIATED CONTENT

Supporting Information

The Supporting Information is available free of charge at https://pubs.acs.org/doi/10.1021/acs.energyfuels.3c01537.

Results from the SOI_{late} and EGR sweeps that are partially shown in Figures 8 and 12 in the main text (PDF)

AUTHOR INFORMATION

Corresponding Author

Jonathan A. Martin − *National Renewable Energy Laboratory (NREL), Golden, Colorado 80401, United States;* orcid.org/0000-0002-1239-6300; Phone: (303) 275-4581; Email: jonathan.martin@nrel.gov

Authors

Matthew A. Ratcliff − *National Renewable Energy Laboratory (NREL), Golden, Colorado 80401, United States;* orcid.org/0000-0001-5616-3317

Mohammad J. Rahimi − *National Renewable Energy Laboratory (NREL), Golden, Colorado 80401, United States;* orcid.org/0000-0002-2688-9456

Jonathan L. Burton − *National Renewable Energy Laboratory (NREL), Golden, Colorado 80401, United States*

Petr Sindler − *National Renewable Energy Laboratory (NREL), Golden, Colorado 80401, United States*

Cameron K. Hays − *National Renewable Energy Laboratory (NREL), Golden, Colorado 80401, United States*

Robert L. McCormick − *National Renewable Energy Laboratory (NREL), Golden, Colorado 80401, United States;* orcid.org/0000-0003-1462-7165

Complete contact information is available at: https://pubs.acs.org/10.1021/acs.energyfuels.3c01537

Author Contributions

The manuscript was written through the contributions of all authors. All authors have given approval to the final version of the manuscript. The main bulk of the manuscript was written by Jonathan Martin, who also generated most of the figures and led the design and execution of the engine experiments. The "Selection of Fuels" section was written by Matthew Ratcliff, who led the selection, design, and blending of the test fuels while executing some of the engine experiments. The "CFD Modeling" section was written by Mohammad Rahimi, who performed the CFD simulations and analysis and generated the associated figures. Jonathan Burton and Petr Sindler constructed the engine experimental setup and executed some of the engine

https://doi.org/10.1021/acs.energyfuels.3c01537
Energy Fuels 2023, 37, 12243−12258

experiments. Cameron Hays performed a chemical analysis of the fuels. Shashank Yellapantula and Robert McCormick provided project guidance and editorial support.

Notes

The authors declare no competing financial interest.

■ ACKNOWLEDGMENTS

This work was authored by the National Renewable Energy Laboratory (NREL), operated by Alliance for Sustainable Energy, LLC, for the U.S. Department of Energy (DOE) under Contract No. DE-AC36-08GO28308. This research was conducted as part of the co-optimization of Fuels and Engines (co-optima) project sponsored by the U.S. DOE's Office of Energy Efficiency and Renewable Energy Bioenergy Technologies Office and Vehicle Technologies Office. Co-Optima is a collaborative project of several national laboratories initiated to simultaneously accelerate the introduction of affordable, scalable, and sustainable biofuels and high-efficiency, low-emission vehicle engines. Work at the National Renewable Energy Laboratory was performed under contract no. DE347AC36-99GO10337. The views expressed in the article do not necessarily represent the views of the DOE or the U.S. Government. The U.S. Government retains and the publisher, by accepting the article for publication, acknowledges that the U.S. Government retains a nonexclusive, paid-up, irrevocable, worldwide license to publish or reproduce the published form of this work, or allow others to do so, for U.S. Government purposes. The conversion of the diesel injector for ACI operation was performed by Exergy Engineering LLC, Grand Rapids, MI.

■ ABBREVIATIONS

ACI = advanced compression ignition
BOB = blendstock for oxygenate blending
CA = crank angle
CAC = charge air cooler
CAD = crank angle degrees
CARB = California Air Resources Board
CAT = catalytic converter
CE = combustion efficiency
CFD = computational fluid dynamics
CI = compression ignition
CoV = coefficient of variation
DOE = Department of Energy
DPF = diesel particulate filter
DVPE = dry vapor pressure equivalent
EGR = exhaust gas recirculation
EPA = Environmental Protection Agency
FTP = Federal test procedure
GDI = gasoline direct injection
HCCI = homogeneous charge compression ignition
HD = heavy-duty
HOV = heat of vaporization
HRR = heat release rate
HTHR = high-temperature heat release
ICE = internal combustion engine
IMEP = indicated mean effective pressure
ITE = indicated thermal efficiency
ITHR = intermediate temperature heat release
LD = light-duty
LHV = lower heating value
LLC = low load cycle
LTHR = low-temperature heat release
MCCI = mixing-controlled compression ignition
MD = medium-duty
MON = motor octane number
MPRR = maximum pressure rise rate
NO_X = nitrogen oxides
OI = octane index
ON = octane number
PM = particulate matter
RI = ringing intensity
RON = research octane number
SCR = selective catalytic reduction
SOI = start of injection
TDC = top dead center
UHC = unburnt hydrocarbons
ULSD = ultra-low sulfur diesel
°aTDC = degrees after top dead center

■ REFERENCES

(1) Pachauri, R. K.; Meyer, L. *Contribution of Working Groups I, II and III to the Fifth Assessment Report of the Intergovernmental Panel on Climate Change; Climate Change 2014: Synthesis Report*; IPCC: Geneva, Switzerland, 2014.
(2) International Energy Agency. *Global EV Outlook 2020*; IEA: Paris, 2020, URL: iea.rg/reports/global-ev-outlook-2020.
(3) Tartaglia, K.; Birky, A.; Laughlin, M.; Price, R. E. A. *Transportation Electrification Beyond Light Duty: Technology and Market Assessment; Report No. ORNL/TM-2017/77-R1*; Oak Ridge National Lab (ORNL), 2017.
(4) International Energy Agency. *The Future of Trucks: Implications for Energy and the Environment*; IEA: Paris, 2017.
(5) Davis, S. J.; Lewis, N. S.; Shaner, M.; Aggarwal, S.; Arent, D.; Azevedo, I. L.; Benson, S. M.; Bradley, T.; Brouwer, J.; Chiang, Y. M.; et al. Net-zero emissions energy systems. *Science* **2018**, *360*, 6396.
(6) Leach, F.; Kalghatgi, G.; Stone, R.; Miles, P. The scope for improving the efficiency and environmental impact of internal combustion engines. *Transport. Eng.* **2020**, *1*, 100005.
(7) Mueller, C. J. *Mixing-Controlled Compression-Ignition Combustion: What it Is Fuel Effects and Prospects for the Future*; Sandia National Laboratory: Albuquerque, NM, 2018, URL: osti.gov/servlets/purl/1495784.
(8) Dec, J. A Conceptual Model of DI Diesel Combustion Based on Laser-Sheet Imaging*. *SAE Trans.* **1997**, *106*, 970873−971348.
(9) Reşitoğlu, İ. A.; Altinişik, K.; Keskin, A. The pollutant emissions from diesel-engine vehicles and exhaust aftertreatment systems. *Clean Technol. Environ. Policy* **2015**, *17*, 15−27.
(10) Burton, J. L.; Martin, J. A.; Fioroni, G. M.; et al. *Fuel Property Effects of a Broad Range of Potential Biofuels on Mixing Control Compression Ignition Engine Performance and Emissions; SAE Technical Paper 2021-01-0505*, 2021.
(11) Dempsey, A. B.; Curran, S. J.; Wagner, R. M. A perspective on the range of gasoline compression ignition combustion strategies for high engine efficiency and low NOx and soot emissions: Effects of in-cylinder fuel stratification. *Int. J. Engine Res.* **2016**, *17*, 897−917.
(12) Dec, J. E.; Dernotte, J.; Ji, C. Increasing the load range, load-to-boost ratio, and efficiency of low-temperature gasoline combustion (LTGC) engines. *SAE Int. J. Engines* **2017**, *10*, 1256−1274.
(13) Cung, K. D.; Ciatti, S. A.; Tanov, S.; Andersson, Ö. Low-Temperature Combustion of High Octane Fuels in a Gasoline Compression Ignition Engine. *Front. Mech. Eng.* **2017**, *3*, 22.
(14) Szybist, J. P.; Splitter, D. A. Impact of engine pressure-temperature trajectory on autoignition for varying fuel properties. *Appl. Energy Combust. Sci.* **2020**, *1*−*4*, 100003−100004.
(15) Thring, R. H. *Homogeneous-Charge Compression-Ignition (HCCI) Engines; SAE Technical Paper 892068*, 1989.

https://doi.org/10.1021/acs.energyfuels.3c01537
Energy Fuels 2023, 37, 12243−12258

(16) Stanglmaier, R. H.; Roberts, C. E. *Homogeneous Charge Compression Ignition (HCCI): Benefits, Compromises, and Future Engine Applications; SAE Technical Paper 1999-01-3682*, 1999.
(17) Dec, J. E. Advanced compression-ignition engines—understanding the in-cylinder processes. *Proc. Combust. Inst.* **2009**, *32*, 2727−2742.
(18) Shibata, G.; Urushihara, T. *Auto-Ignition Characteristics of Hydrocarbons and Development of HCCI Fuel Index; SAE Technical Paper 2007-01-0220*, 2007.
(19) Truedsson, I.; Cannella, W.; Johansson, B.; Tuner, M. *Development of New Test Method for Evaluating HCCI Fuel Performance; SAE Technical Paper 2014-01-2667*, 2014.
(20) Cung, K.; Ciatti, S. A Study of Injection Strategy to Achieve High Load Points for Gasoline Compression Ignition (GCI) Operation. *Proceedings of the ASME 2017 Internal Combustion Engine Division Fall Technical Conference*; American Society of Mechanical Engineers: Seattle, Washington, 2017.
(21) Dernotte, J.; Dec, J.; Ji, C. *Efficiency Improvement of Boosted Low-Temperature Gasoline Combustion Engines (LTGC) Using a Double Direct-Injection Strategy; SAE Technical Paper 2017-01-0728*, 2017.
(22) Heywood, J. B. *Internal Combustion Engine Fundamentals*; McGraw-Hill: New York, 1988; pp 71−72.
(23) Wolk, B.; Chen, J.-Y.; Dec, J. E. Computational study of the pressure dependence of sequential auto-ignition for partial fuel stratification with gasoline. *Proc. Combust. Inst.* **2015**, *35*, 2993−3000.
(24) Pintor, D. L.; Dec, J.; Gentz, G. *Φ-Sensitivity for LTGC Engines: Understanding the Fundamentals and Tailoring Fuel Blends to Maximize This Property; SAE Technical Paper 2019-01-0961*, 2019.
(25) Luecke, J.; Zigler, B. T. Rapid prediction of fuel research octane number and octane sensitivity using the AFIDA constant-volume combustion chamber. *Fuel* **2021**, *301*, 120969.
(26) Martin, J. A.; Burton, J. L.; Luecke, J.; McCormick, R. L. *Impacts of Biofuel Blending on MCCI Ignition Delay with Review of Methods for Defining Cycle-by-Cycle Ignition Points from Noisy Cylinder Pressure Data; SAE Technical Paper 2021-01-0497*, 2021.
(27) Ortiz-Soto, E. A.; Lavoie, G. A.; Martz, J. B.; Wooldridge, M. S.; Assanis, D. N. Enhanced heat release analysis for advanced multi-mode combustion engine experiments. *Appl. Energy* **2014**, *136*, 465−479.
(28) Pintor, D. L.; Dec, J.; Gentz, G. Experimental Evaluation of a Custom Gasoline-Like Blend Designed to Simultaneously Improve ϕ-Sensitivity, RON and Octane Sensitivity. *SAE Int. J. Adv. Curr. Pract. Mobility* **2020**, *2*, 2196−2216.
(29) Senecal, P. K.; Richards, K. J.; Pomraning, E.; Yang, T.; Dai, M. Z.; McDavid, R. M.; Patterson, M. A.; Hou, S.; Shethaji, T. *A New Parallel Cut-Cell Cartesian CFD Code for Rapid Grid Generation Applied to in-Cylinder Diesel Engine Simulations; SAE Technical Paper 2007-01-0159*, 2007.
(30) NIST/TRC Web Thermo Tables (WTT). https://wtt-pro.nist.gov/wtt-pro, 3/8/21.
(31) Luecke, J.; Rahimi, M. J.; Zigler, B. T.; Grout, R. W. Experimental and numerical investigation of the Advanced Fuel Ignition Delay Analyzer (AFIDA) constant-volume combustion chamber as a research platform for fuel chemical kinetic mechanism validation. *Fuel* **2020**, *265*, 116929.
(32) DieselNet. United States: Heavy-Duty Onroad Engines: California Low NOx Regulation, 2022. https://dieselnet.com/standards/us/hd.php#lownox (accessed June 12, 2022).
(33) Messerly, R. A.; Luecke, J. H.; St John, P. C.; Etz, B. D.; Kim, Y.; Zigler, B. T.; McCormick, R. L.; Kim, S. Understanding how chemical structure affects ignition-delay-time φ-sensitivity. *Combust. Flame* **2021**, *225*, 377−387.
(34) Dagle, V. L.; Affandy, M.; Lopez, J. S.; Cosimbescu, L.; Gaspar, D. J.; Scott Goldsborough, S.; Rockstroh, T.; Cheng, S.; Han, T.; Kolodziej, C. P.; Hoth, A.; Majumdar, S. S.; Pihl, J. A.; Alleman, T. L.; Hays, C.; et al. Production, fuel properties and combustion testing of an iso-olefins blendstock for modern vehicles. *Fuel* **2022**, *310*, 122314.
(35) Chatterjee, T.; Saggese, C.; Dong, S.; Patel, V.; Lockwood, K.; Curran, H.; Labbe, N.; Wagnon, S.; Pitz, W. Experimental and kinetic modeling study of the low- temperature and high-pressure combustion chemistry of straight chain pentanol isomers: 1-2- and 3-Pentanol. *Proc. Combust. Inst.* **2023**, *39*, 265−274.

https://doi.org/10.1021/acs.energyfuels.3c01537
Energy Fuels 2023, 37, 12243−12258